Journal of the Mechanics and Physics of Solids 123 (2019) 305–314

Contents lists available at ScienceDirect

Journal of the Mechanics and Physics of Solids

journal homepage: www.elsevier.com/locate/jmps

Plasticity retards the formation of creases

Jiawei Yang[a,b], Lihua Jin[a,c], John W. Hutchinson[a], Zhigang Suo[a,*]

[a] John A. Paulson School of Engineering and Applied Sciences, Kavli Institute for Nanobio Science and Technology, Harvard University, Cambridge, MA 02138, United States
[b] School of Aerospace Engineering and Applied Mechanics, Tongji University, Shanghai 200092, China
[c] Department of Mechanical and Aerospace Engineering, University of California, Los Angeles, CA 90095, United States

ARTICLE INFO

Article history:
Received 28 June 2018
Revised 21 August 2018
Accepted 22 August 2018
Available online 25 August 2018

Keywords:
Creases
Plasticity
Hysteresis
Metal
Plastics

ABSTRACT

When an elastomer is compressed, its surface forms creases at a critical strain about 0.35. When a plastically deformable material is compressed, however, its surface remains smooth at much larger strains. As the smooth surface folds locally into a crease, the material around the crease loads and unloads. We show that the hysteresis of plasticity retards the formation of the crease. For a crease growing in an infinite body, the stress field is self-similar as the crease grows, and the critical strain ϵ^c is the applied strain needed to maintain the self-similar growth. We simulate the formation of creases using an elastic-plastic model with linear hardening, and characterize the degree of plasticity of the model by the ratio of the tangent modulus to elastic modulus, E_t/E. A small value of E_t/E leads to a large critical strain for the onset of creases. We further show experimentally that creases can form at a strain of 0.49 for high-density polyethylene (HDPE) with $E_t/E \sim 0.025$, but cannot form for metals (aluminum, copper, and stainless steel) with $E_t/E \sim 0.001$.

1. Introduction

When an elastomer is compressed beyond a critical strain, its surface folds locally into self-contact and forms a crease (Fig. 1a). Further compression increases the length of self-contact. Upon unloading, the crease unfolds continuously until the surface becomes smooth again. At the level of strains when the crease forms, most elastomers are well described by the neo-Hookean model, which is characterized by a single material parameter, the shear modulus. At the onset of the crease, the length of the self-contact is small compared to lengths characterizing the specimen. Consequently, the critical strain for the onset of crease is a constant, independent of the type, size and shape of the elastomer, and independent of the method of loading.

About two decades ago, the critical strain for the onset of crease was found experimentally to be 0.35 (Gent and Cho, 1999). These authors could not reconcile this experimental value with the critical strain 0.46 predicted theoretically for the onset of smooth surface wrinkles (Biot, 1965), but their basic experimental findings have been amply confirmed by other researchers. In experiments of homogeneous elastomers under compression, smooth surface wrinkles have never been reported, but creases have been reported widely (Barros et al., 2012; Cai et al., 2010, 2011; Dervaux and Amar, 2012; Ghatak and Das, 2007; Hong et al., 2009; Saha et al., 2010; Tanaka et al., 1992, 1987; Trujillo et al., 2008; Weiss et al., 2013; Yoon et al., 2010). Creases can be triggered in many ways (Li et al., 2012), on a hydrogel under compression (Hong et al., 2009) (Fig. 1b), on a hydrogel swelling under constraint (Tanaka et al., 1987; Trujillo et al., 2008; Yoon et al., 2010) (Fig. 1c), on a

* Corresponding author.
E-mail address: suo@seas.harvard.edu (Z. Suo).

https://doi.org/10.1016/j.jmps.2018.08.016
0022-5096/

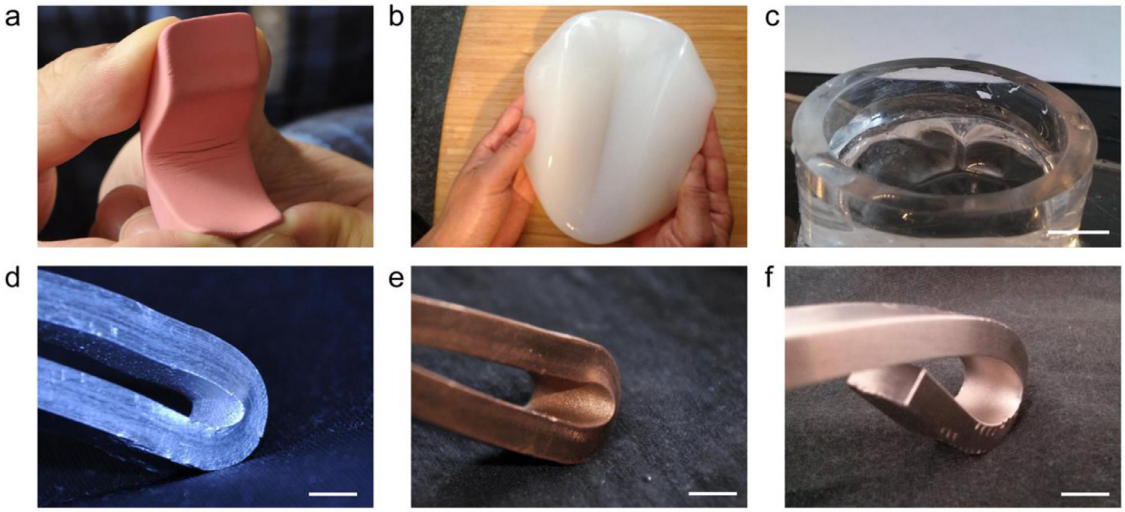

Fig. 1. Under compression, gels and elastomers form creases, but metals do not. Creases form on the surfaces of (a) an eraser, (b) Liang Fen (a starch gel, a popular Chinese food, courtesy of Denian Zhuang), and (c) a swollen hydrogel. Creases do not form on the surfaces of (d) aluminum, (e) copper, and (f) stainless steel. The scale bar is 5 mm.

tissue growing under constraint (Dervaux et al., 2011; Jin et al., 2011), on an elastomer under compression (Cai et al., 2011; Saha et al., 2010), and on a dielectric elastomer under electric field (Wang et al., 2012; Wang et al., 2011).

Creases affect various functions in biology and engineering. Gyri form as a human brain matures (Richman et al., 1975; Tallinen et al., 2016); The formation of creases is also commonly observed during the swelling of a constrained hydrogel, and this phenomenon has been suggested to mimic tumor growth (Dervaux et al., 2011). Creases can be used to develop a surface that reversibly hides and exposes surface under temperature change (Kim et al., 2010), and that functions as a mechanically gated electrical switch (Xu et al., 2014). However, undesirable creases need to be avoided because they may damage materials. Creases in walls of tires subjected to large bending deformation may lead to earlier failure (Gent and Cho, 1999). Creases formed in the adaptive lens may significantly change the focal length (Zalachas et al., 2013).

The fundamental study of creases took a decisive turn when it was pointed out that creases and wrinkles are two distinct types of instability (Hohlfeld and Mahadevan, 2011, 2012). For the convenience of wording, consider an elastomer undergoing homogeneous deformation. In either type of instability, the homogeneous deformation becomes unstable and gives way to inhomogeneous deformation. At the transition, the inhomogeneous state deviates from the homogeneous state by a perturbation, which is *infinitesimal* in some sense. Wrinkles set in by a perturbation of *infinitesimal strain*. By contrast, a crease sets in by a perturbation of large strain, but *infinitesimal length of self-contact*. Once a spatially-localized, large-amplitude perturbation is introduced on the surface, the calculated critical strain for the onset of crease is around 0.35. The creased state has lower elastic energy than the homogeneous state (Hong et al., 2009; Jin et al., 2015, 2011; Jin et al., 2014). Finite element simulations have shown that wrinkles are unstable and dynamically collapse to creases (Cao and Hutchinson, 2011). If defects on the surface are small, surface energy is a barrier to creasing, and will increase the critical strain for the onset of a crease (Chen et al., 2012). The formation of creases can become complex when they form on the surface of a substrate with gradient modulus or with pre-compression (Chen et al., 2014; Diab et al., 2013).

So far, the literature has been devoted exclusively to creases on materials capable of large elastic deformation (e.g., elastomers, gels, and tissues). Here we study creases on materials capable of large plastic deformation (e.g., metals and plastics). Our preliminary experiment has shown that when metal bars are bent, the inner surfaces remain smooth at strains much beyond 35% (Figs. 1d–f). When a smooth surface locally folds into a crease, the material around the crease loads and unloads. For a plastically deformable material, loading and unloading exhibit hysteresis, which dissipates energy. We hypothesize that plasticity retards the formation of a crease, in a way analogous to that plasticity retards the growth of a crack. When the contact length is small compared to other lengths, the crease is in effect growth in an infinite body, and the contact length is the only relevant length scale. Once the distance is normalized by the contact length, as the crease grows, the stress field is *self-similar*. The applied strain needed to maintain the self-similar growth defines the critical strain e^c for the onset of the crease. We use the finite element method to simulate the growth of creases in materials capable of large plastic deformation, and show that the hysteresis of plasticity increases the critical strain for the onset of crease. We perform crease tests on several materials, including aluminum 6061, copper 101, stainless steel, and high-density polyethylene. The combination of computation and experiment supports the hypothesis that plasticity retards the formation of creases.

To provide further perspective, recall several types of instability commonly observed in plastically deformable materials. When a sheet of metal deforms plastically, the homogeneous state may bifurcate into an inhomogeneous state

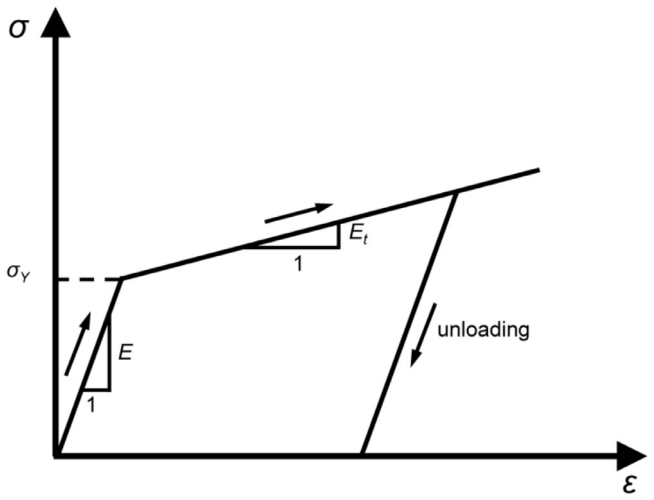

Fig. 2. Loading and unloading stress-strain curve of an elastic-plastic material model with linear hardening.

(Needleman and Rice, 1978; Rice, 1976; Stören and Rice, 1975; Young, 1976). Examples include Lüders bands (Hallai and Kyriakides, 2011; Lubliner, 2008), shear bands (Anand and Spitzig, 1980; Hutchinson and Tvergaard, 1981; Needleman and Rice, 1978; Rice, 1973, 1976; Rudnicki and Rice, 1975), and surface wrinkles (Hutchinson and Tvergaard, 1980; Larsson et al., 1982; Triantafyllidis, 1980). Surface wrinkles are observed on a pressurized aluminum alloy tube near fracture region, and on a bent carbon steel tube also with a small strain (Hallai and Kyriakides, 2011; Larsson et al., 1982). For these instabilities, bifurcation analysis is often used to calculate the critical strain, which is found strongly depends on the elasto-plastic constitutive laws (Anand and Spitzig, 1980; Hutchinson and Tvergaard, 1980, 1981; Needleman and Rice, 1978; Rudnicki and Rice, 1975). No crease has ever been experimentally observed or theoretically predicted in plastic materials, perhaps because these materials develop other types of instability before reaching the critical strain for creases. Creases have been observed in a plastic film on a compliant substrate (Cao et al., 2012), and on the surface of bulk thermoplastics through ultrahigh electric fields (Wang et al., 2012). However, the effect of plasticity on the formation of creases has not been studied before.

2. Finite element simulation

To study the effect of plasticity on the formation of creases by finite element simulation, we need to choose a material model. The material model must capture an essential aspect of plasticity: the state of stress depends on the history of the state of strain, not just on the final state of strain. Beyond this aspect of plasticity, in this paper we choose not to study other more refined aspects of plasticity. We adopt the J_2 flow theory with linear hardening (Fig. 2). This elastic-plastic model involves four material properties: Young's modulus E, Poisson's ratio ν, initial yield strength σ_Y, and tangent modulus E_t. All these properties are taken to be constant, independent of plastic deformation.

The critical strain e^c for the onset of creases is a function of three dimensionless parameters: E_t/E, σ_Y/E, and ν. Because creases form at large strains, the effect of elastic compressibility is negligible, and we do not study the effect of Poisson's ratio ν. The value of E_t/E is bounded between 0 and 1. When $E_t/E=1$, the model becomes a purely elastic model with no hysteresis. As E_t/E decreases, the hysteresis increases. When $E_t/E=0$, the model becomes an ideal plastic model. We expect that e^c increases as E_t/E decreases. Similarly, we expect that e^c increases as σ_Y/E decreases, but our simulation will show that e^c is much less sensitive to σ_Y/E than to E_t/E. Incidentally, σ_Y/E sets the size of elastic strain, which is much smaller than the strain at which creases form. We further assume that the defects on the surfaces are large enough, so that the effect of surface energy is negligible. Thus, this material model reduces the study of the effect of plasticity on creasing to the problem of computing e^c as a function of E_t/E.

We use the commercial finite element software Abaqus 6.10/Standard to simulate the formation of a crease under plane strain conditions. The computational model is a rectangular block subject to a compressive strain $e=(H-h)/H$, where H is the length in the undeformed state, and h is the length in the deformed state (Fig. 3a). When the strain is beyond a critical value e^c, the material block forms a crease (Fig. 3b). We characterize the size of the crease by the length of self-contact, l. The material properties (E, E_t and σ_Y) are determined using the diagram of true stress and natural strain, $\varepsilon=\ln(1-e)$.

We follow the finite element method used to analyze creases on an elastomer (Cai et al., 2011). Instead of focusing on the initiation of a crease, this approach calculates the *growth* of a crease as the applied compressive strain increases. Due to symmetry, we simulate the left half of the block, size $H\times H$ in the undeformed state. The size of the block affects the growth of deep creases, but not the onset of creases. A quarter of a small circular defect is prescribed at the intersection of the free surface and symmetrical boundary, with radius of the defect is $D\sim H/1000$, far smaller than the thickness of the block. To resolve the stress and strain fields near the defect, the size of the mesh near the defect is far smaller than the size

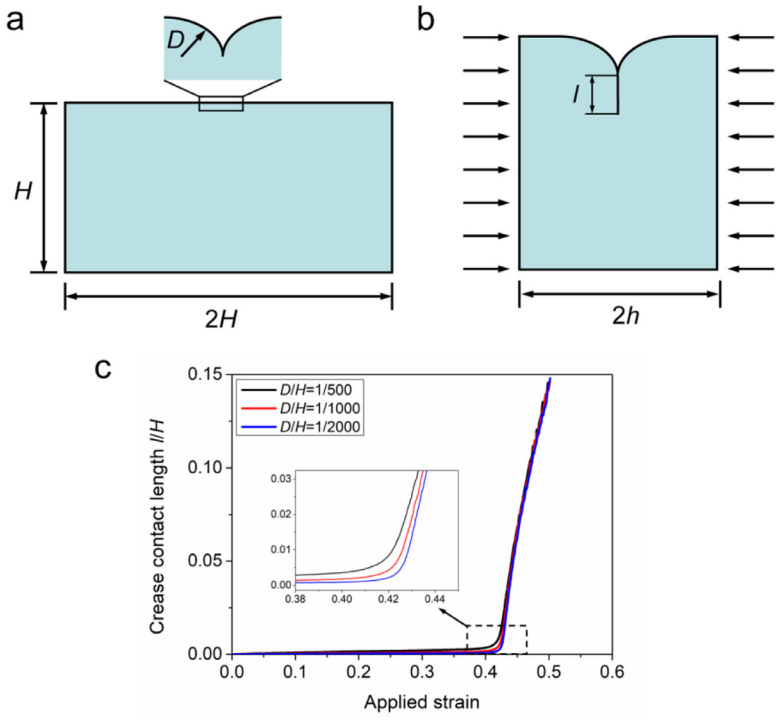

Fig. 3. Computational model. (a) A block of material is of height H and width $2H$ in the reference state. A defect is introduced on the surface by placing together two quarters of a circle with radius D. (b) The block is compressed to width $2h$, and the surface forms a crease with the self-contact length l. The applied strain is defined as $e=(H-h)/H$. (c) Crease contact length l/H evolves with the applied strain for several defect sizes. Here, $E_t/E=0.6$ and $\sigma_Y/E=0.005$.

of the defect. A uniform horizontal displacement is prescribed on the left boundary. The right boundary is the symmetric boundary. On the bottom boundary, the vertical displacement is constrained, and the horizontal displacement is free. The block is meshed with 4-node bilinear plane strain quadrilateral CPE4 elements.

The computational model has two length scales: the size D of the defect and the size H of the block. We assume that the two length scales are widely separated: $D<<H$. To illustrate the effect of the defect size, we simulate the formation of crease for several values of D/H (1/2000, 1/1000 and 1/500). We track the contact length l as the applied strain e increases (Fig. 3c). The defect size slightly affects the l–e curve when the contact length is comparable to the defect size, but does not affect the l-e curve when the contact length is much larger than the defect size. A smaller defect gives a steeper increase of the contact length at initiation. As $D/H\to 0$, the l–e curve is expected to intersect the horizontal axis vertically. We determine the critical strain for the onset of crease when the contact length increases steeply. So long as the two length scales are widely separated, $D<<H$, the defect size negligibly affects the critical strain, which is about ~0.42 for all three curves.

We examine the evolution of the field as the applied strain changes (Movie S1 for more details of the evolution). The material on the free surface far from the crease is homogeneously compressed. As a material particle enters the crease region, the curved surface of the crease stretches and thus unloads the material particle, which is shown by the decreasing principal compressive strain on the free surface toward the crease (Fig. 4a). This loading and unloading behavior near the crease causes pronounced hysteresis.

When the applied strain reaches 0.51, we reduce the applied strain. The crease gradually unfolds, but the surface does not become smooth even when the applied force vanishes. A V-shaped morphology remains on the free surface with substantial residual stress (Fig. 4b). This residual crease is associated with plastic deformation, and is different from unloading a crease in an elastomer. A larger E_t/E gives a shallower V-shape. When $E_t/E=1$, the material model becomes purely elastic, and the surface of unloaded block becomes flat. This behavior is consistent with the unloading of a creased elastomer.

We also track the evolution of the state of a representative material particle P as the applied strain changes. This evolution is characterized by several parameters: the principal compressive strain (Fig. 4c), the orientation (Fig. 4d), and the ratio of the in-plane maximum principal stress to the in-plane minimum principal stress (Fig. 4e). Four representative states (1), (2), (3), (4) are marked on the stress-strain curve, corresponding to loading, unloading, re-loading, and unloading again (Fig. 4f).

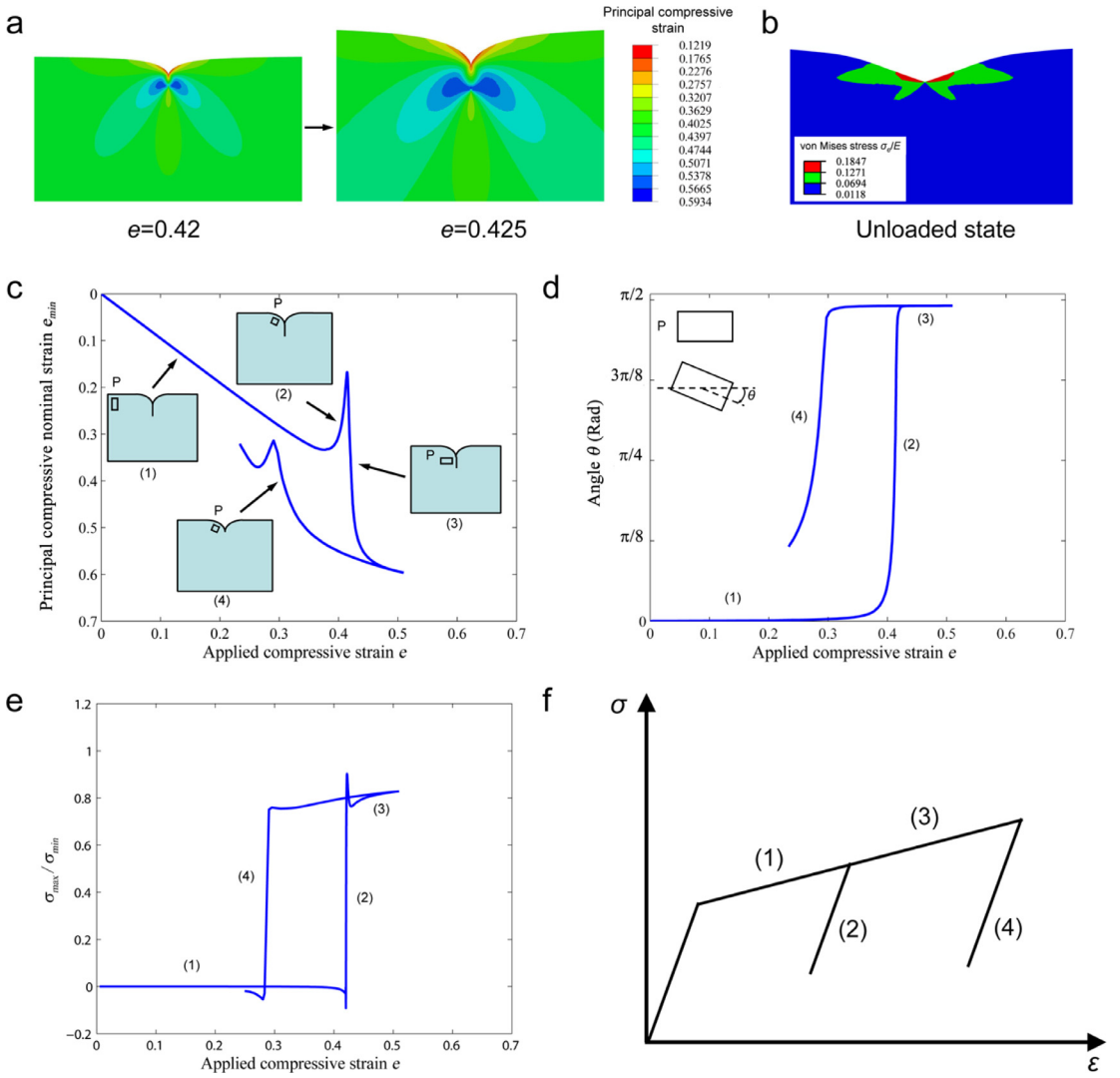

Fig. 4. Evolution of a crease during loading and unloading. (a) A crease evolves from $e=0.42$ to 0.425. Note that as the applied strain increases, the principal strain on the free surface decreases towards the crease, which implies unloading in the crease. (b) Unloading after the applied strain reaches 0.51. The crease unfolds but does not vanish and leave a V-shaped residual morphology. When the applied strain increases, the state of a material particle P evolves. This evolution is characterized by several parameters: (c) the principal compressive strain of particle P, (d) the orientation of particle P, and (e) the ratio of the in-plane maximum principal stress to the in-plane minimum principal stress. (f) Four states (1)–(4) are marked on the stress-strain curve. The calculation is obtained from simulation with $E_t/E=0.6$, $\sigma_Y/E=0.005$, and $D/H=0.001$.

In state (1), the material particle P is far away from the defect, and is in a region under homogeneous deformation. The principal strain coincides with the applied strain (Fig. 4c), and the principal orientation is parallel to the loading direction, $\theta=0$ (Fig. 4d). The material particle P is under proportional loading, $\sigma_{\max}/\sigma_{\min}=0$ (Fig. 4e).

In state (2), the material particle P has already entered the curved surface of the crease. The principal strain of particle P decreases as the applied strain increases (Fig. 4c). The material particle P rotates 90 degrees towards the crease contact region (Fig. 4d). This rotation causes non-proportional loading, $\sigma_{\max}/\sigma_{\min}>0$ (Fig. 4e).

In state (3), the material particle P is in the crease contact region. The principal strain increases as the applied strain increases (Fig. 4c), and the principal orientation maintains perpendicular to the loading direction (Fig. 4d). The material particle P is still under non-proportional loading (Fig. 4e).

In state (4), the material particle P is unloaded. The material particle P first moves towards the free surface in the contact region, and finally settles down on the free surface. The principal strain decreases (Fig. 4c), and the principal orientation settles down to a finite value of 22.5° (Fig. 4d). This final angle defines the sharpness of V-shaped residual crease.

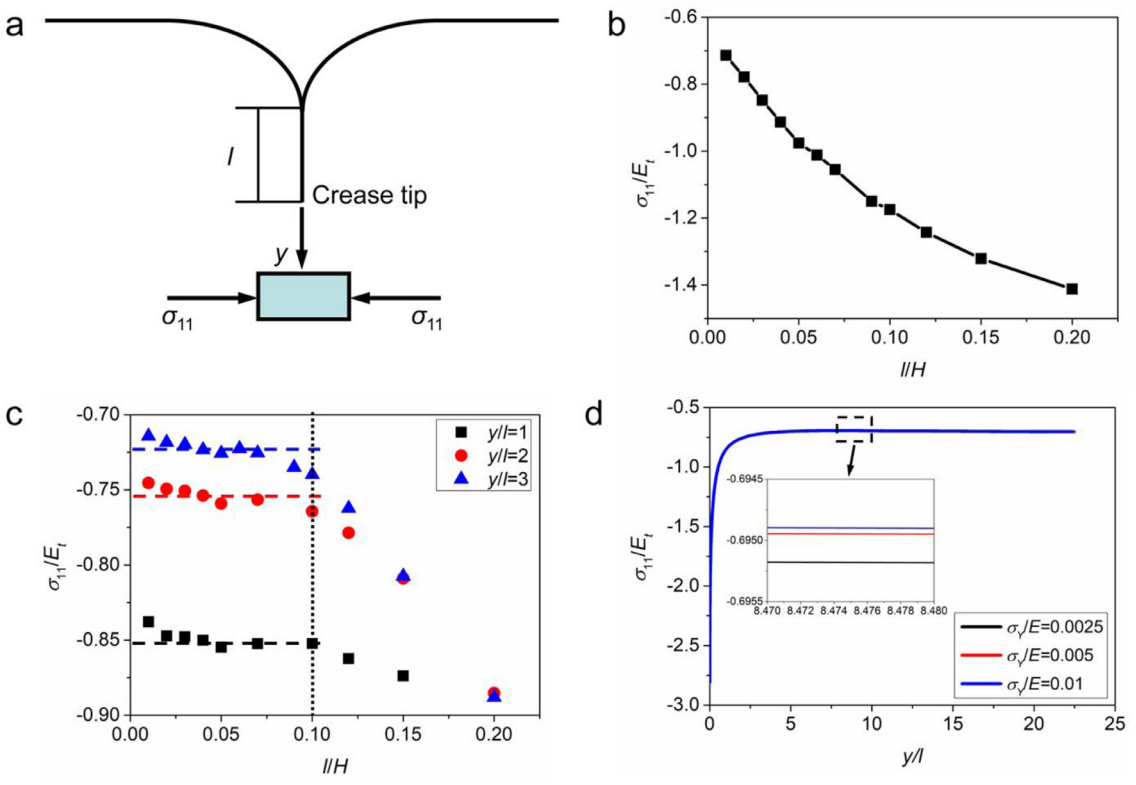

Fig. 5. Self-similar evolution of a crease. (a) Schematic of a material particle located in a distance y below the crease tip. The stress σ_{11} is tracked as the crease grows. (b) The stress σ_{11} as a function of crease contact length for material particles fixed at $y/D = 30$. (c) The stress σ_{11} as a function of crease contact length for material particles located at $y/l = 1$, 2 and 3. (d) For a fixed contact length $l/H = 0.06$, the stress σ_{11} as a function of y/l with various yield strengths. All three curves fall into a single curve, negligibly dependent on the yield strength. Calculations are done for $E_t/E = 0.6$, $\sigma_Y/E = 0.005$ and $D/H = 0.001$.

3. Self-similar growth of a crease

The growth of a crease is analogous to the blunting of a crack in that they both evolve by self-similar fields. For an infinitely long crack blunting in an infinitely large body, the crack opening displacement is the only length scale. As the crack opening displacement increases, the stress field is self-similar when the distance is normalized by the crack-tip opening displacement (McMeeking, 1977). Similarly, for a crease growing in an infinitely large body, the contact length is the only length scale. As the contact length increases, the stress field is self-similar when the distance is normalized by the contact length. The critical strain e^c is the applied strain needed to maintain the self-similar growth of the crease. In the following, we use finite element simulation to first show that the formation of a crease is self-similar.

Our numerical simulation only approximately realizes the self-similarity because the computational model has two additional length scales, D and H. We define a coordinate y with the origin at the crease tip (Fig. 5a). As the contact length l increases, the origin of the y axis moves, and a sequence of material particles pass the spatial point of coordinate y. We calculate the distribution of the horizontal stress σ_{11} (y). If the spatial point is at a fixed distance from the crease tip, $y/D = 30$, σ_{11} drops significantly as the contact length grows (Fig. 5b). If the spatial point is at a distance that scales with the contact length, $y/l =$ constant, σ_{11} maintains approximately a constant value when $D < l < 0.1\ H$ (Fig. 5c). When $l < D$, the defect affects the stress. When $l > 0.1H$, the size of the block affects the stress. In both cases, the σ_{11} changes as the contact length increases, and the growth is not self-similar. For an infinitesimally small defect and infinitely large body, the evolution of a crease should be exactly self-similar.

We further show that the stress state near the crease tip weakly depends on the initial yield strength. We fix a crease contact length $l/H = 0.06$ and calculate the stress σ_{11} at different y/l with three values of the initial yield strength. All three curves almost fall into a single curve. This is because significant plastic deformation has evolved the stress level far beyond its initial value. The independence of stress state and initial yield strength is also observed in HRR field (Hutchinson, 1968; Rice and Rosengren, 1968). Also note that when y/l is above ~5, the stress reaches a plateau, which implies that the stress state in this region is unaffected by the growth of crease.

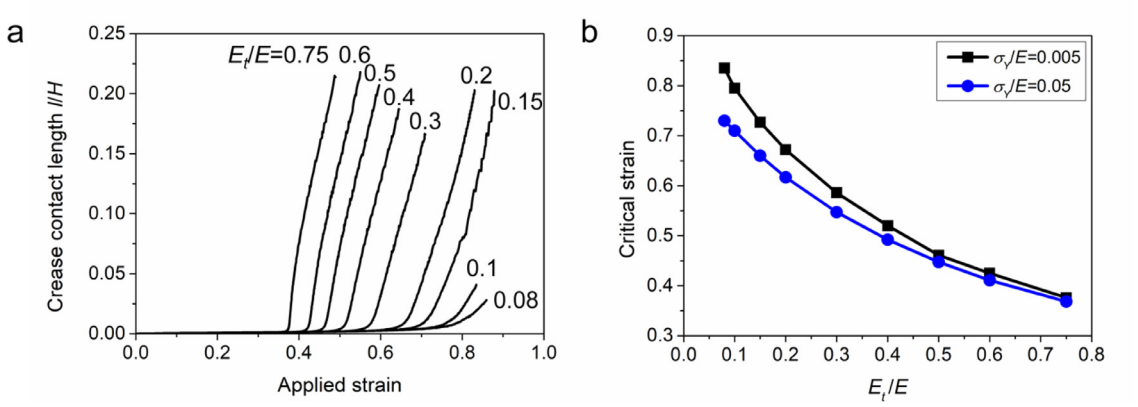

Fig. 6. The critical strain for the onset of a crease. (a) The normalized contact length l/H as functions of the applied strain at different values of E_t/E. $\sigma_Y/E = 0.005$ and $D/H = 0.001$ are used in the calculations. (b) The critical strain for the onset of crease decreases as E_t/E increases, and is less sensitive to the value of σ_Y/E.

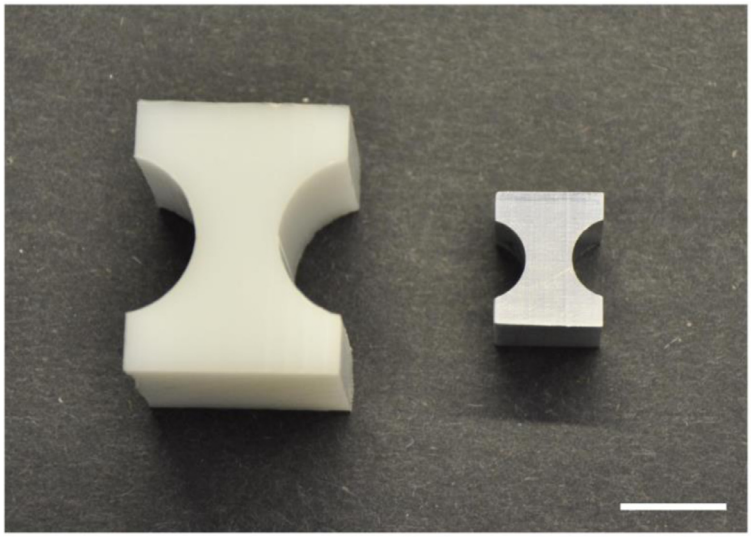

Fig. 7. The design of specimens for the crease tests. Left: high-density polyethylene. Right: aluminum. The scale bar is 1 cm.

4. The critical strain for the onset of a crease

As noted before, the ratio of the tangent modulus to the elastic modulus measures the degree of plasticity of the material model. We plot the normalized contact length l/H as a function of the applied strain e for various values of E_t/E (Fig. 6a). Recall that the strain for the surface to self-contact depends on the defect size D introduced in the computational model. Also recall that a crease undergoes self-similar growth in an infinite body, and that the critical strain e^c is the applied strain needed to maintain the self-similar growth. In the numerical simulation, we determine e^c as the applied strain when the contact length increases steeply. The uncertainty introduced by this practice is small so long as the two length scales separate widely, $D << H$.

As expected, a smaller E_t/E gives a larger critical strain e^c for creases (Fig. 6b). This trend is understood as follows. A smaller E_t/E exhibits larger hysteresis and larger energy dissipation upon unloading in the crease region. Consequently, an additional compressive strain is required to initiate the crease. When $E_t/E = 0.75$, the critical strain is ~0.374, very close to the critical strain in elastomers. As $E_t/E \to 1$, the critical strain is expected to be smaller. In contrast, when $E_t/E = 0.08$, the critical strain is ~0.85. Most metals and plastics have E_t/E on this order of magnitude or smaller. At this level of strain, plastic materials may already develop into other forms of localizations, or even rupture. As $E_t/E \to 0$, the material flows plastically after initial elastic deformation. The small elastic energy stored in the material is insufficient to trigger creases, and the critical strain should approach 1. Moreover, at each value of E_t/E, the critical strain for $\sigma_Y/E = 0.05$ is smaller than that for $\sigma_Y/E = 0.005$. This is because larger σ_Y/E recovers more elastic energy upon unloading, and thus facilitates a crease to form earlier. The numerical results indicate that the critical strain is sensitive to E_t/E, but is much less sensitive to σ_Y/E.

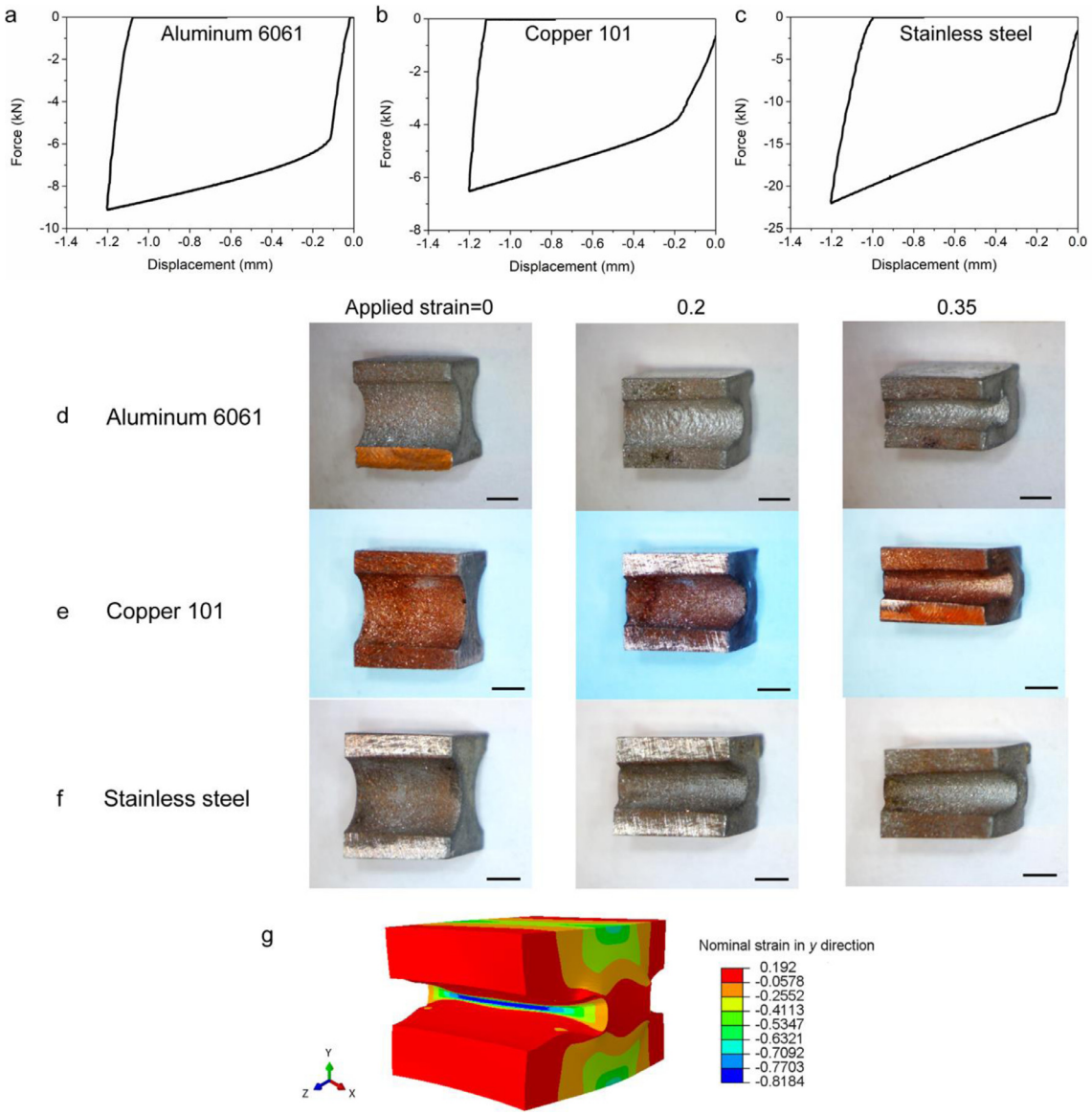

Fig. 8. No crease forms in metals. Loading-unloading force displacement curves of (a) aluminum 6061, (b) copper 101 and (c) stainless steel. The values of E_t/E for all three metals is ~0.001. (d)–(f) Photos of metal specimens at different applied strain. No crease is observed in all three metals. The scale bar is 2 mm. (g) The local strain at the center of the specimen is calculated over 0.8 when the applied strain is 0.35.

5. Crease tests on metals and plastics

Numerical computation, such as the one presented above, depends on the choice of material model. No material model captures all nuances of plasticity of metals and plastics. The predictions on the basis of any material model should be used with caution. To further ascertain our hypothesis that plasticity retards the formation of creases, we conduct experiments using commonly available materials capable of large plastic deformation: aluminum, copper, steel, and high-density polyethylene.

The crease tests for soft elastic materials (e.g., gels, elastomers) typically include bending test (Gent and Cho, 1999; Ghatak and Das, 2007; Hohlfeld and Mahadevan, 2011) and uniaxial compression test by releasing a pre-stretched elastic substrate (Cai et al., 2011). Direct compression test is often impractical, because at large compression, the specimen is likely to bulge out on the lateral surfaces due to the friction at the top and bottom surfaces, even with lubricant. It is also impractical to find a substrate to compress metals and plastics to a large strain. To address the testing issues, here we design a specimen of a special shape (Fig. 7). The specimen is suitable to mount on a test machine, circumvents the bulging effect, and can induce large compressive strain on both curved surfaces. We use an Instron hydraulic test machine (model 8501)

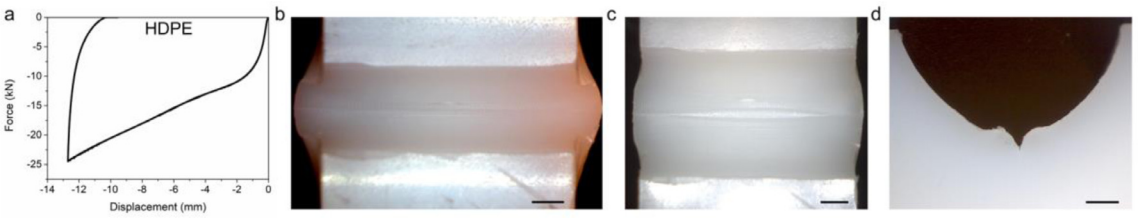

Fig. 9. A crease forms in high-density polyethylene. (a) Loading-unloading force displacement curve of HDPE. The specimen conducted in the test is of rectangular shape with dimensions 1.9 cm × 1.9 cm × 2.54 cm. The value of E_t/E is ~0.025. (b) Photo of a crease on a HDPE specimen at an applied strain of 0.317. The crease extends through the entire surface. (c) Photo of the specimen after unloading. A large opening is observed on the free surface. (d) Cross-sectional view of the opening. A V-shaped morphology of the residual crease is revealed. The scale bar is 2.5 mm.

to perform all the tests. Displacement control is used to track the overall applied strain (displacement divided by the height of the specimen). The loading rate is set at 2.5 mm/min. To identify the critical condition of creases, a digital camera is used to monitor the surface. We perform the crease tests on several metals (aluminum 6061, copper 101 and stainless steel).

To identify the plastic hysteresis of each material, loading and unloading force-displacement curve of each material is measured individually. The loading and unloading force-displacement curves of three metals show drastic plastic hysteresis, and E_t/E are estimated ~0.001 (values are estimated from true stress-strain curves which are converted from the experimentally measured engineering stress-strain curves, so that they can compare with the values predicted by the simulations) (Fig. 8a–c). As the strain is applied up to 0.35, no crease is observed, and the curved surfaces remain smooth (Fig. 8d–f). We conduct finite element simulation to calculate the local strain at the center of the curved surface. We build a computational model of same geometry of specimen, and mesh with 8-node linear brick C3D8. We apply compressive strain to the model and determine the vertical strain field. When the applied strain is 0.35, the local strain is calculated to be ~0.8 (Fig. 8g). We note that at this level of strain, assuming no other localizations set in, the critical strain for creases is predicted much larger than 0.8 when $E_t/E \sim 0.001$ (Fig. 6b). For real metals, also note that the E_t/E value typically is not a constant, and the E_t/E value decreases as the plastic strain increases. Hence, the critical strain for the onset of crease is expected to be even larger.

We further test plastics, since plastics can have larger E_t/E than metals. We measure the loading and unloading force-displacement curve for high-density polyethylene (HDPE) (McMaster-Carr) (the specimen conducted in the test is of rectangular shape with dimensions 1.9 cm × 1.9 cm × 2.54 cm) and estimate $E_t/E \sim 0.025$ (Fig. 9a). The crease test shows that creases form at the center of both curved surfaces at a critical applied strain of 0.208. The corresponding local strain is calculated ~0.498. The crease extends through the entire surface and becomes clear at an applied strain of 0.317 (Fig. 9b). Note that the local critical strain of 0.498 at $E_t/E \sim 0.025$ is inconsistent with the prediction of our numerical simulation (Fig. 6b). The cause of this discrepancy is unclear at this writing.

We subsequently unload the specimen. The crease gradually unfolds but does not vanish and leave a large opening (Fig. 9c). The cross-sectional view of the opening reveals a V-shaped morphology (Fig. 9d), which is consistent with the result of numerical simulation (Fig. 4b).

6. Conclusion

In summary, our computation and experiment have shown that plasticity retards the formation of creases. As the surface forms a crease, a material particle near the crease evolves by a complex sequence of states: loading when the particle is far from the crease region, unloading when the particle enters the crease region, and re-loading when the particle is in the self-contact region. The loading-unloading hysteresis dissipates energy and retards the growth of the crease. For a crease growing in an infinite body, the stress field is self-similar once the distance is normalized by the contact length. The applied strain needed to maintain the self-similar growth defines the critical strain for the onset of the crease.

We simulate the formation of a crease using a material model that captures an essential aspect of plasticity: the state of stress depends on the history of the state of strain. Within this model, the degree of plasticity is characterized by the ratio of the tangent modulus to elastic modulus E_t/E. A smaller value of E_t/E exhibits more pronounced hysteresis, and thereby leads to a larger critical strain for the onset of crease. Upon unloading, the crease unfolds and leaves a *V*-shaped morphology on the free surface due to the irreversible plastic deformation. A crease forms on a HDPE with $E_t/E = 0.025$ at a critical strain of ~0.498, larger than 0.35 which is the critical strain in elastomers with no hysteresis. However, no crease forms on metals with $E_t/E \sim 0.001$ even at a strain of 0.8.

Acknowledgment

Work at Harvard was supported by MRSEC (DMR-14-20570). Yang was supported by China Scholarship Council as a visiting scholar for two years at Harvard University. We thank Prof. Joost Vlassak for the use of Instron Hydraulic test machine

(model 8501). We also thank Steve Sansone of Laboratory for Particle Physics and Cosmology at Harvard University for machining the specimens.

Reference

Anand, L., Spitzig, W., 1980. Initiation of localized shear bands in plane strain. J. Mech. Phys. Solids 28, 113–128.
Barros, W., de Azevedo, E.N., Engelsberg, M., 2012. Surface pattern formation in a swelling gel. Soft Matter 8, 8511.
Biot, M.A., 1965. Mechanics of Incremental Deformation. John Wiley and Sons, New York.
Cai, S., Bertoldi, K., Wang, H., Suo, Z., 2010. Osmotic collapse of a void in an elastomer: breathing, buckling and creasing. Soft Matter 6, 5770–5777.
Cai, S., Chen, D., Suo, Z., Hayward, R.C., 2011. Creasing instability of elastomer films. Soft Matter 8, 1301–1304.
Cao, Y.-P., Zheng, X.-P., Jia, F., Feng, X.-Q., 2012. Wrinkling and creasing of a compressed elastoplastic film resting on a soft substrate. Comput. Mater. Sci. 57, 111–117.
Cao, Y., Hutchinson, J.W., 2011. From wrinkles to creases in elastomers: the instability and imperfection-sensitivity of wrinkling. Proc. R. Soc.-Math. Phys. Eng. Sci. 468, 94–115.
Chen, D., Cai, S., Suo, Z., Hayward, R.C., 2012. Surface energy as a barrier to creasing of elastomer films: an elastic analogy to classical nucleation. Phys. Rev. Lett. 109 038001-038001.
Chen, D., Jin, L., Suo, Z., Hayward, R.C., 2014. Controlled formation and disappearance of creases. Mater. Horiz. 1, 207–213.
Dervaux, J., Amar, M.B., 2012. Mechanical Instabilities of Gels. Annu. Rev. Condens. Matter Phys. 3, 311–332.
Dervaux, J., Couder, Y., Guedeau-Boudeville, M.A., Ben Amar, M., 2011. Shape transition in artificial tumors: from smooth buckles to singular creases. Phys. Rev. Lett 107, 018103.
Diab, M., Zhang, T., Zhao, R., Gao, H., Kim, K.S., 2013. Ruga mechanics of creasing: from instantaneous to setback creases. Proc. R. Soc. A 469, 20120753.
Gent, A.N., Cho, I.S., 1999. Surface instabilities in compressed or bent rubber blocks. Rubber Chem. Technol. 72, 253–262.
Ghatak, A., Das, A.L., 2007. Kink instability of a highly deformable elastic cylinder. Phys. Rev. Lett. 99.
Hallai, J.F., Kyriakides, S., 2011. On the effect of lüders bands on the bending of steel tubes. Part I: Experiments. Int. J. Solids Struct. 48, 3275–3284.
Hohlfeld, E., Mahadevan, L., 2011. Unfolding the Sulcus. Phys. Rev. Lett. 106.
Hohlfeld, E., Mahadevan, L., 2012. The sacle and nature of sulcification patterns. Phys. Rev. Lett. 109.
Hong, W., Zhao, X.H., Suo, Z.G., 2009. Formation of creases on the surfaces of elastomers and gels. Appl. Phys. Lett. 95.
Hutchinson, J., 1968. Singular behaviour at the end of a tensile crack in a hardening material. J. Mech. Phys. Solids 16, 13–31.
Hutchinson, J.W., Tvergaard, V., 1980. Surface instabilities on statically strained plastic solids. Int. J. Mech. Sci. 22, 339–354.
Hutchinson, J.W., Tvergaard, V., 1981. Shear band formation in plane-strain. Int. J. Solids Struct. 17, 451–470.
Jin, L., Auguste, A., Hayward, R.C., Suo, Z., 2015. Bifurcation diagrams for the formation of wrinkles or creases in soft bilayers. J. Appl. Mech. 82, 061008.
Jin, L., Cai, S., Suo, Z., 2011. Creases in soft tissues generated by growth. Epl 95.
Jin, L., Chen, D., Hayward, R.C., Suo, Z., 2014. Creases on the interface between two soft materials. Soft Matter 10, 303–311.
Kim, J., Yoon, J., Hayward, R.C., 2010. Dynamic display of biomolecular patterns through an elastic creasing instability of stimuli-responsive hydrogels. Nat. Mater. 9, 159–164.
Larsson, M., Needleman, A., Tvergaard, V., Stroakers, B., 1982. Instability and failure of internally pressurized ductile metal cylinders. J. Mech. Phys. Solids 30, 121–154.
Li, B., Cao, Y.-P., Feng, X.-Q., Gao, H., 2012. Mechanics of morphological instabilities and surface wrinkling in soft materials: a review. Soft Matter 8, 5728–5745.
Lubliner, J., 2008. Plasticity Theory. Courier Corporation.
McMeeking, R.M., 1977. Finite deformation analysis of crack-tip opening in elastic-plastic materials and implications for fracture. J. Mech. Phys. Solids 25, 357–381.
Needleman, A., Rice, J., 1978. Limits to ductility set by plastic flow localization. Mechanics of Sheet Metal Forming. Springer.
Rice, J., Rosengren, G., 1968. Plane strain deformation near a crack tip in a power-law hardening material. J. Mech. Phys. Solids 16, 1–12.
Rice, J.R., 1973. The initiation and growth of shear bands. In: Palmer, A.C (Ed.), Proceedings of the Symposium on the Role of Plasticity in Soil Mechanics, Cambridge, England, pp. 263–274.
Rice, J.R., 1976. The localization of plastic deformation. In: Koiter, W.T (Ed.), Proceedings of the14th International Congress on Theoretical and Applied Mechanics. North Holland Publishing Co, Delft, pp. 207–220.
Richman, D.P., Stewart, R.M., Hutchinson, J., Caviness, V., 1975. Mechanical mode of brain convolutional development. Science 189, 18–21.
Rudnicki, J.W., Rice, J., 1975. Conditions for the localization of deformation in pressure-sensitive dilatant materials. J. Mech. Phys. Solids 23, 371–394.
Saha, K., Kim, J., Irwin, E., Yoon, J., Momin, F., Trujillo, V., Schaffer, D.V., Healy, K.E., Hayward, R.C., 2010. Surface creasing instability of soft polyacrylamide cell culture substrates. Biophys. J. 99, L94–L96.
Stören, S., Rice, J.R., 1975. Localized necking in thin sheets. J. Mech. Phys. Solids 23, 421–441.
Tallinen, T., Chung, J.Y., Rousseau, F., Girard, N., Lefèvre, J., Mahadevan, L., 2016. On the growth and form of cortical convolutions. Nat. Phys.
Tanaka, H., Tomita, H., Takasu, A., Hayashi, T., Nishi, T., 1992. Morphological and kinetic evolution of surface patterns in gels during the swelling process: evidence of dynamic pattern ordering. Phys. Rev. Lett 68, 2794–2797.
Tanaka, T., Sun, S.T., Hirokawa, Y., Katayama, S., Kucera, J., Hirose, Y., Amiya, T., 1987. Mechanical instability of gels at the phase-transition. Nature 325, 796–798.
Triantafyllidis, N., 1980. Bifurcation phenomena in pure bending. J. Mech. Phys. Solids 28, 221–245.
Trujillo, V., Kim, J., Hayward, R.C., 2008. Creasing instability of surface-attached hydrogels. Soft Matter 4, 564–569.
Wang, Q., Niu, X., Pei, Q., Dickey, M.D., Zhao, X., 2012. Electromechanical instabilities of thermoplastics: theory and in situ observation. Appl. Phys. Lett. 101, 141911–141914.
Wang, Q., Zhang, L., Zhao, X., 2011. Creasing to cratering instability in polymers under ultrahigh electric fields. Phys. Rev. Lett. 106.
Weiss, F.o., Cai, S., Hu, Y., Kyoo Kang, M., Huang, R., Suo, Z., 2013. Creases and wrinkles on the surface of a swollen gel. J. Appl. Phys. 114, 073507.
Xu, B., Chen, D., Hayward, R.C., 2014. Mechanically gated electrical switches by creasing of patterned metal/elastomer bilayer films. Adv. Mater. 26, 4381–4385.
Yoon, J., Kim, J., Hayward, R.C., 2010. Nucleation, growth, and hysteresis of surface creases on swelled polymer gels. Soft Matter 6, 5807–5816.
Young, N., 1976. Bifurcation phenomena in the plane compression test. J. Mech. Phys. Solids 24, 77–91.
Zalachas, N., Cai, S., Suo, Z., Lapusta, Y., 2013. Crease in a ring of a pH-sensitive hydrogel swelling under constraint. Int. J. Solids Struct. 50, 920–927.